

© 2021 IEEE. Personal use of this material is permitted. Permission from IEEE must be obtained for all other uses, in any current or future media, including reprinting/republishing this material for advertising or promotional purposes, creating new collective works, for resale or redistribution to servers or lists, or reuse of any copyrighted component of this work in other works.

Digital Object Identifier [10.1109/ECCE47101.2021.9595531](https://doi.org/10.1109/ECCE47101.2021.9595531)

2021 IEEE Energy Conversion Congress and Exposition (ECCE)

Design Oriented Analysis of Control Loops Interaction in Power Synchronization-based Voltage Source Converter

Federico Cecati

Marco Liserre

Yicheng Liao

Xiongfei Wang

Frede Blaabjerg

Suggested Citation

F. Cecati, M. Liserre, Y. Liao, X. Wang and F. Blaabjerg, "Design Oriented Analysis of Control Loops Interaction in Power Synchronization-based Voltage Source Converter," 2021 IEEE Energy Conversion Congress and Exposition (ECCE), 2021.

Design Oriented Analysis of Control Loops Interaction in Power Synchronization-based Voltage Source Converter

Federico Cecati and Marco Liserre
Chair of Power Electronics
Kiel University
Kiel, Germany
fc@tf-uni.kiel.de, ml@tf-uni.kiel.de

Yicheng Liao, Xiongfei Wang and Frede Blaabjerg
Department of Energy Technology
Aalborg University
Aalborg, Denmark
ycl@et.aau.dk, xwa@et.aau.dk, fbl@et.aau.dk

Abstract—Power synchronization mechanism is coupled with the dc-link, since both synchronization and dc-link dynamics depend on the active power. The active power filter used in the frequency droop is correlated with inertia emulation, which affects the dc-link voltage. Furthermore, the coupling between active and reactive power in the low-voltage grid suggests a possible interaction between dc-link and reactive power control. The strong coupling between all the control loops and the dc-link in power synchronization-based converters represents a challenge both for the stability and for the controller tuning. This paper addresses the tuning of power synchronization-based converter with consideration of all the control loops interactions. A complete converter state-space model is derived, and a step-by-step tuning procedure based on eigenvalue analysis is proposed. Experimental results are provided to demonstrate the method.

Index Terms—Power Synchronization, DC Voltage Control, State-Space Modeling

I. INTRODUCTION

Power synchronization in Voltage Source Converters (VSCs) aims to emulate the dynamics of Synchronous Generators (SGs), and it is employed both in grid forming converters [1] and in VSC connected to very weak grid [2], [3]. Nevertheless, while in the SG the active power fluctuations reflect on the rotor kinetic energy, in voltage source converters (VSCs) they reflect on the dc capacitor electrical energy [1], [4]. The dc-link dynamics and the control have therefore a great influence on the power converter behavior, and may interact with other control loops. This paper considers a power synchronization-based converter with dc voltage control implemented in the grid side converter, as in Fig. 1 [2], [3].

The authors gratefully acknowledge the funding by Deutsche Forschungsgemeinschaft (DFG, German Research Foundation) via the Priority Program DFG SPP 1984 “Hybrid and Multimodal Energy Systems” and by Gesellschaft für Energie und Klimaschutz Schleswig-Holstein GmbH (EKSH) doctoral studies grant.

The control loop interaction mechanisms are shown in Fig. 2. The $P - \omega$ droop (in red) varies the frequency to adjust the active power, whose variation affects the dc voltage control (in yellow). However, the frequency droop often employs a low-pass filter on the active power, which has been demonstrated to emulate the inertia [4], [5]. The inertia emulation further affects the dc voltage control, since it results in active power exchange with the dc bus [1], [6]. Several papers in literature have already highlighted the strict relation between frequency and dc-link voltage [1], [4]–[6], but none of them provided a state-space model to study the dynamic behavior and tune the control loops accordingly. L. Zhang *et al.* proposed in [2] the power synchronization loop for VSC-HVDC systems including the dc voltage control, and later in 2019 a tuning guideline was given for it [3]. Yet, the focus of these researches is on the power synchronization loop, and not on its interactions with other loops, e.g. the reactive power loop.

The resistive-inductive nature of the low voltage grid impedance results in a coupling between active and reactive power droops, as highlighted by the green arrows in Fig. 2 [7]. The reactive power regulation process (in violet) is therefore coupled with the active power, and can influence the dc voltage. The coupling between dc-link dynamics and reactive power loop in power synchronization has so far been not investigated in literature.

The complexity of the interaction mechanisms between the dc-link dynamics and all the control loops represents a great challenge for the tuning. The choice of the control gains has to be based on a complete model including all the control loops in order to take into account all the possible interactions. The paper [8] proposed a tuning method for multi-loop systems, nevertheless it did not consider the dc-link dynamics.

This paper derives a complete state-space model of

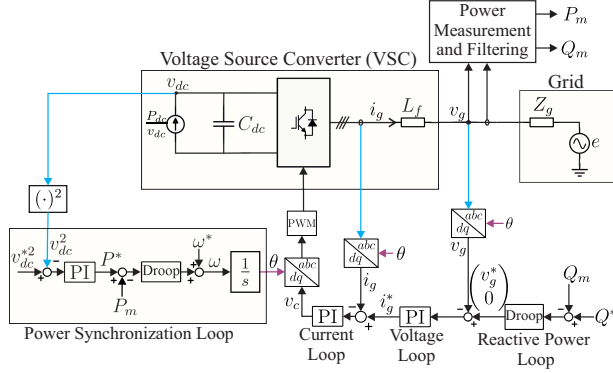


Figure 1: The considered power converter control scheme with active power synchronization loop.

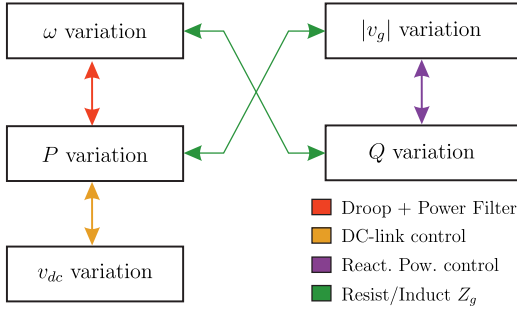


Figure 2: The interaction mechanism between the different control loops.

a power synchronization-based converter, including the dc-link dynamics [9]–[11]. From the derived model, a step-by-step tuning procedure involving the dynamical interactions of six control loops is proposed, based on eigenvalue analysis. Simulation and experimental results validate the proposed tuning procedure.

II. SYSTEM DESCRIPTION AND MODELING

The considered VSC control scheme, depicted in Fig. 1, presents a power synchronization loop as given in [2], and a reactive droop control cascaded with a double voltage-current loop, similar to [12]. The presence of the current loop enhances the converter current limitation capability [13]. The active/reactive power low-pass filtering, which is relevant for inertia emulation, is shown in Fig. 1 [5]. The considered converter presents an L-filter L_f , motivated by the increasing interest in L-filtered MMCs in converters with inertia emulation [14]–[16]. The lack of the output ac capacitor makes the state-space modeling as well as the double voltage-current loop design challenging [10], [14]. The papers [9], [10] proposed to model the inverter and its current loop $G_{cc}(s) = K_p + \frac{K_i}{s}$ with the state-space representation of its impedance model to break through this limit. The

model of the current loop is given:

$$\begin{cases} \dot{v}_{cc} = K_i i_c - K_i i_g \\ \dot{i}_c = -\frac{K_p}{L_f} i_c + \frac{K_p}{L_f} i_g^* \\ v_g = K_p (i_c - i_g) + v_{cc} \end{cases} \quad (1)$$

where v_{cc} and i_c are auxiliary state variables to express the output voltage v_g , according to [10].

The model in (1) can be merged with the model of the voltage loop, power synchronization loop, reactive power loop, and dc-link dynamics, to form the complete nonlinear state-space model of the converter shown in Fig. 1 by the form:

$$\dot{x} = f(x) + g(x) \begin{pmatrix} e \\ P_{dc} \end{pmatrix} \quad (2)$$

where the inputs are the grid voltage e and the active power P_{dc} , which are considered as disturbances. The nonlinear model is:

$$\begin{cases} \dot{i}_c = -\frac{K_p}{L_f} i_c + \frac{K_p}{L_f} i_g^* \\ \dot{\Phi}_g = v_g^* - v_g \\ \dot{v}_{dc}^2 = -\frac{3}{2} \frac{1}{C_{dc}} v_g^T i_g + \frac{1}{C_{dc}} P_{dc} \\ \dot{\Phi}_{dc} = v_{dc}^2 - v_{dc}^{*2} \\ \dot{P}_m = -\omega_f P_m + \omega_f v_g^T i_g \\ \dot{Q}_m = -\omega_f Q_m + \omega_f v_g^T \begin{pmatrix} 0 & -1 \\ 1 & 0 \end{pmatrix} i_g \\ \dot{\delta} = -m_p (P_m - P^*) \\ \dot{v}_{cc} = -K_i i_g + K_i i_c \\ \dot{i}_g = \frac{R_g}{L_g} i_g - \Omega i_g + \frac{1}{L_g} (v_g - T(\delta)e) \end{cases} \quad (3)$$

with

$$\begin{cases} v_g = K_p (i_c - i_g) + v_{cc} \\ v_g^* = \begin{pmatrix} V_n - n_q (Q_m - Q^*) \\ 0 \end{pmatrix} \\ P^* = K_{p_{dc}} (v_{dc}^2 - v_{dc}^{*2}) + K_{i_{dc}} \Phi_{dc} \\ i_g^* = K_{p_v} (v_g^* - v_g) + K_{i_v} \Phi_g \\ T(\delta) = \begin{pmatrix} \cos \delta & \sin \delta \\ -\sin \delta & \cos \delta \end{pmatrix} \\ \Omega = \begin{pmatrix} 0 & -\omega \\ \omega & 0 \end{pmatrix} \end{cases} \quad (4)$$

ω_f is the power filter time constant, V_n is the ac nominal voltage, m_p is the P - ω droop gain, n_q is the Q - V droop gain, $K_{p_{dc}}$ and $K_{i_{dc}}$ the dc voltage control gains, K_{p_v} and K_{i_v} the ac voltage control gains and Φ_{dc} , Φ_v the integral states of dc and ac voltage control, respectively. The model in (2) is linearized obtaining:

$$\dot{x} = Ax + B \begin{pmatrix} e \\ P_{dc} \end{pmatrix} \quad (5)$$

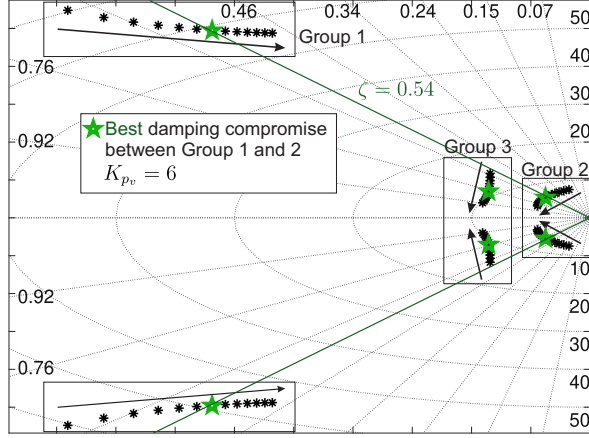


Figure 3: Tuning procedure for the voltage loop. Arrows indicate increasing K_{pv} .

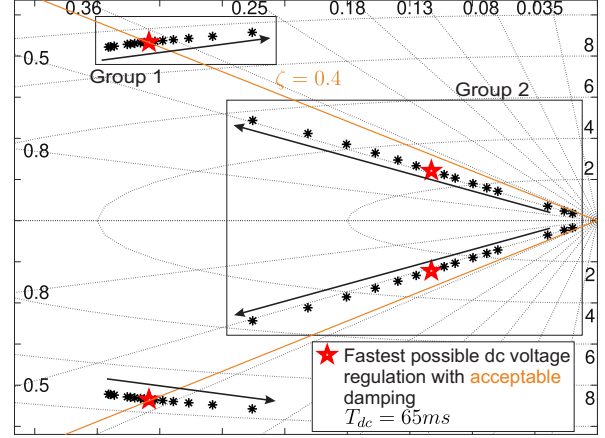


Figure 5: Tuning procedure for the dc voltage control. Arrows indicate increasing K_{pdc} .

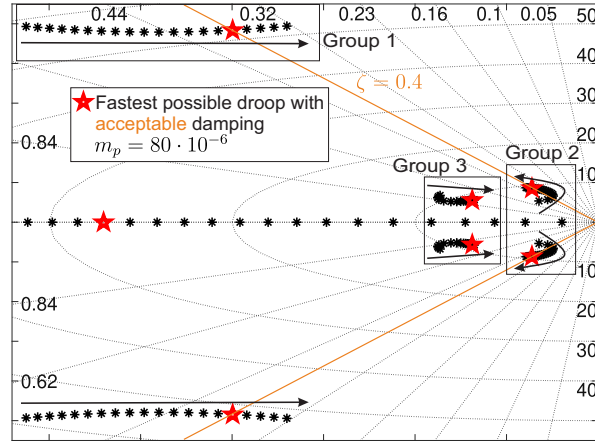


Figure 4: Tuning procedure for the frequency droop. Arrows indicate increasing m_p .

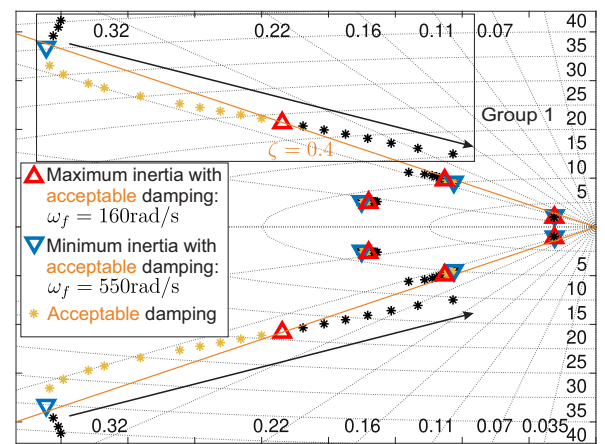


Figure 6: Tuning procedure for the active power filter for inertia emulation. Arrows indicate increasing inertia (decreasing ω_f).

III. STEP-BY-STEP TUNING PROCEDURE

The proposed tuning method is based on the eigenvalues of the linearized model (5). The model parameters are set according to Table I. Since (5) includes the dynamics of all the control loops, all the eventual

interactions are taken into account in the tuning. The procedure follows the research onion philosophy [17]: in the first step only the most internal loops are tuned and the external ones are not considered. Afterwards, the external loops are added and tuned one-by-one, considering the well-tuned internal loops designed in the previous steps. The eigenvalue analysis is used at each

Table I: Simulation parameters for the power synchronization-based converter

Parameters	Values
Line-to-line grid voltage e (V)	690
Short Circuit Ratio of Z_g	1.5
R/X ratio of Z_g	0.3
Nominal active power P_{dc} (MW)	2
Nominal dc-link voltage v_{dc}^* (V)	1200
Switching frequency (kHz)	2
DC-link capacitor C_{dc} (mF)	22
Filter inductor L_f (mH)	0.1

Table II: Experimental tests VSC and grid hardware parameters

Parameters	Values
Line-to-line grid voltage e (V)	400
Short Circuit Ratio of Z_g	2.5
R/X ratio of Z_g	0.3
Nominal active power P_{dc} (kW)	10
Nominal dc-link voltage v_{dc}^* (V)	800
Switching frequency (kHz)	10
DC-link capacitor C_{dc} (mF)	1.2
Filter inductor L_f (mH)	5.5

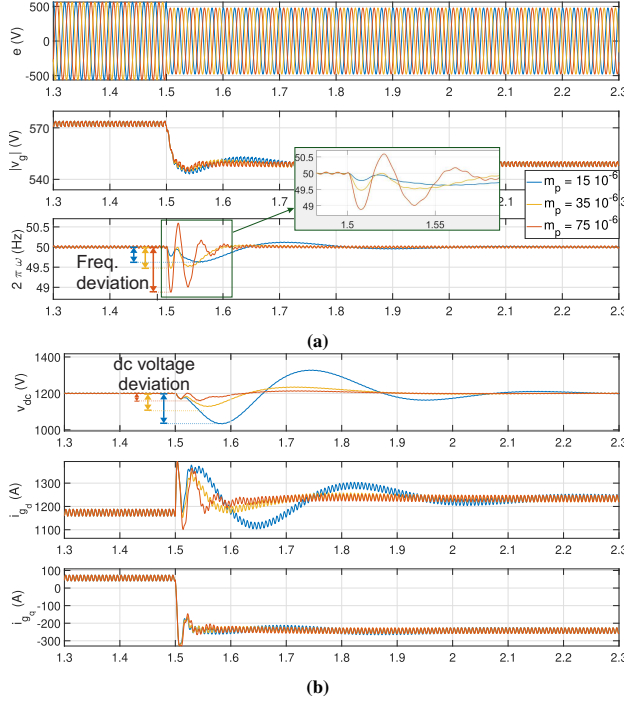


Figure 7: The simulation results under different values of the frequency droop gain. (a) Grid voltage, converter voltage amplitude and frequency. (b) DC-link voltage, active and reactive current.

tuning step to analyze the converter dynamics and to adjust the control parameters in order to obtain the best dynamical and damping performances. The proposed tuning procedure ensures a minimal eigenvalue damping of 0.4, evaluated on the complete VSC model including all the control loops. According to a control theory result in [18], a minimum eigenvalue damping of 0.4 in the time-domain corresponds to a 45 deg phase margin in frequency domain, resulting in good robustness.

The order in which the control loops are tuned, highlighted in the following step-by-step procedure, has a fundamental importance. The proposed procedure has six steps:

- 1) The current loop is the first to be designed, and it is tuned through the well-established technical optimum rule [19].
- 2) Afterwards, the voltage loop is added to the current loop model, and it is tuned according to the system eigenvalues with the considered SCR and R/X ratio, declared in Table I. The PI voltage controller time constant T_v is first chosen ten times greater than the inner current loop time constant, therefore $K_{iv} = \frac{K_{pv}}{T_v}$. The proportional gain K_{pv} is initialized to 0 and increased until the eigenvalues of groups 1 and 2 of Fig. 3 reach the same damping as highlighted by the green line. The optimal tuning is highlighted with the green star in Fig. 3.

- 3) The droop gain m_p is initially tuned according to the rule on the maximum frequency deviation $m_p = \frac{\Delta\omega}{P_{nom}}$ [20]. Afterward, m_p is increased until the eigenvalues of groups 1 in Fig. 4 reach the critical damping $\zeta = 0.4$, highlighted by the orange line. The resulting tuning ensures fast synchronization with high stability margin, and is highlighted by the red star in Fig. 4.
- 4) The dc-link voltage control is initially tuned in order to produce a reference power which is able to balance the stored dc-link energy deviation in a defined time constant T_{dc} , chosen initially relatively large (e.g. 400 ms). With this rule, $K_{pdc} = \frac{1}{2}C_{dc}\frac{1}{T_{dc}}$ and $K_{idc} = \frac{K_{pdc}}{T_{dc}}$. From this initial tuning, T_{dc} is decreased (K_{pdc}, K_{idc} increased) until the damping of the group 1 in Fig. 5 reaches a critical value $\zeta = 0.4$ highlighted by the orange line. The resulting tuning ensures a fast dc voltage tracking, low dc voltage transient deviation and high stability margin, and is highlighted by the red star in Fig. 4.
- 5) The reactive power loop is added, and n_q is initially tuned according to the voltage deviation rule $n_q = \frac{\Delta V}{2Q_{max}}$ [20].
- 6) The active power filter cutoff frequency, inversely proportional to the emulated inertia [5], is tuned as the last loop, thus with consideration of all the control loops interactions (including the reactive power loop). ω_f is initialized very high (no inertia), and then it is progressively decreased to give more virtual inertia; the eigenvalues of group 1 in Fig. 6 cross the critical damping orange line twice. According to the analysis in Fig. 6, the value of ω_f can be chosen between 160 rad/s and 550 rad/s depending on the desired inertia emulation, always keeping a good and robust system stability ($\zeta > 0.4$).

IV. SIMULATION RESULTS

The considered power converter in Fig. 1 is modeled and simulated in MATLAB/Simulink[®] environment; the simulation parameters are summarized in Table I. A symmetrical voltage sag of 0.15 p.u. with a phase jump of 10 degrees is applied to the grid voltage e . Target of the simulations is to validate the converter dynamics behavior predicted by the eigenvalue analyses in section III.

The first simulation in Fig. 7 illustrates the converter behavior under different values of the frequency droop gain m_p . By increasing m_p , the frequency tracked by the converter has a higher deviation from its nominal value and higher Rate of Change of Frequency (RoCoF), in accordance with the literature [20]. Additionally, the frequency profile shows low-damped oscillations which severely affect the system stability. The frequency of

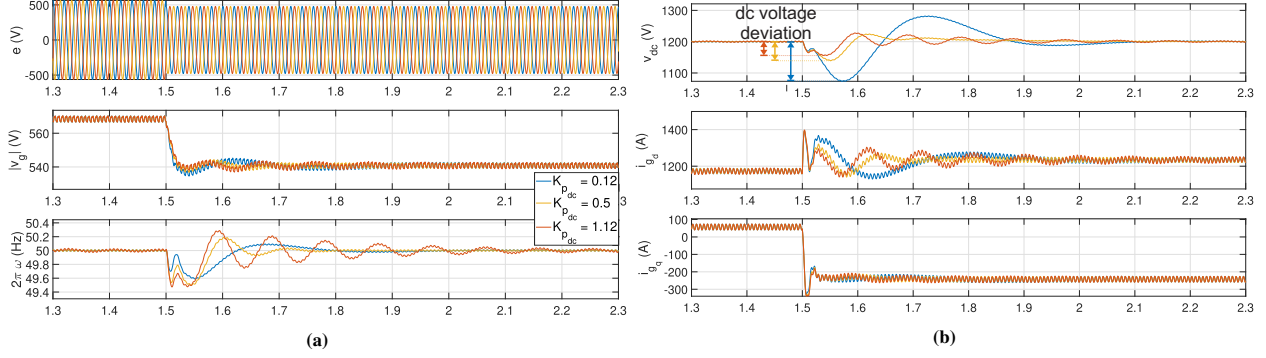


Figure 8: The simulation results under different values of the dc voltage control proportional gain. (a) Grid voltage, converter voltage amplitude and frequency. (b) DC-link voltage, active and reactive current.

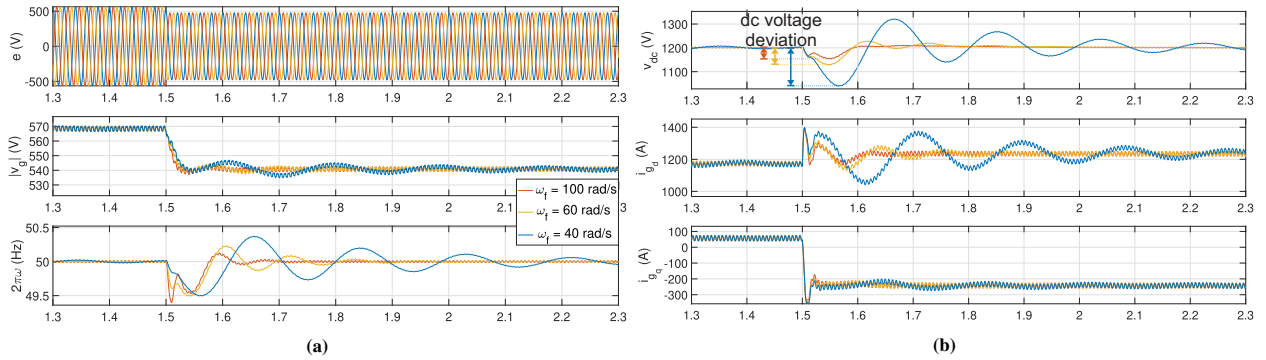


Figure 9: The simulation results under different values of the active power filter bandwidth. (a) Grid voltage, converter voltage amplitude and frequency. (b) DC-link voltage, active and reactive current.

Table III: Experimental results control parameter tuning

Parameter/ Case study	$K_{p,dc}$	$K_{i,dc}$	m_p	n_q	ω_f	K_{pv}	K_{iv}
Fig. 11(a)	0.025	0.1	0.0031	0.00015	60	1	300
Fig. 11(b)	0.001	0.06	0.0021	0.0001	60	1.2	350
Fig. 11(c)	0.025	0.15	0.0041	0.00005	45	1	300
Fig. 11(d) (proposed method)	0.015	0.1	0.0031	0.0001	100	1.5	400

these oscillations is between 50 and 60 Hz, as predicted by the eigenvalue analysis in Fig. 4. The simulation in Fig. 4(b) reveals a strong influence of this parameter on the dc voltage dynamics as well, which indeed is controlled by varying the converter frequency. With low values of m_p , the dc voltage has large and slow oscillations. This result is in accordance with [5]: the parameter m_p in droop controlled VSCs is inversely proportional to the inertia coefficient in Virtual Synchronous Machine. A high emulated inertia (low m_p) results in higher power exchange with the dc-link, resulting in large dc voltage oscillations.

The analysis with respect to the dc-link controller proportional gain is shown in Fig. 8. This parameter impacts the overall system dynamics similarly to the parameter m_p , albeit with a lower influence on the RoCoF and maximum frequency deviation. Moreover,

the oscillations in Fig. 8(a) generated by high values of $K_{p_{dc}}$ have a frequency which is lower (around 25 Hz) respect to the case of Fig. 7(a), in accordance with the eigenvalue analyses of Figs. 4 and 5. According to the proposed tuning procedure, $K_{p_{dc}}$ has to be chosen as high as possible; the reason of this choice becomes more clear in Fig. 8(b). When $K_{p_{dc}}$ is low, the dc voltage control action is weak: even if the oscillations are well damped as correctly predicted by Fig. 5, they result in a high deviation from the nominal value which can potentially cause overmodulation phenomena and/or damage on the semiconductor devices.

The analysis depending on the power filter cut-off frequency ω_f , is shown in Fig. 9. The parameter ω_f is inversely proportional to the emulated inertia [5]. By decreasing ω_f (increasing the emulated inertia), the frequency dip is indeed slowed down and the RoCoF is

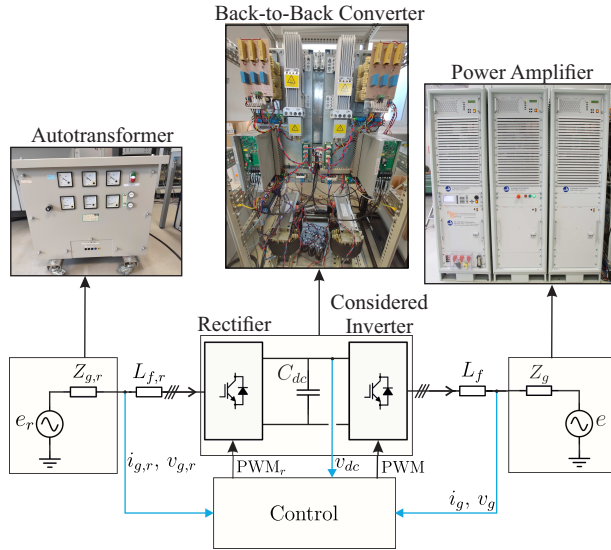


Figure 10: The experimental setup configuration.

decreased. As a drawback, inertia emulation results in a high power exchange with the dc-link, which results in large dc voltage oscillations. Moreover, differently from the previous cases of Figs. 7 and 8, the dc voltage oscillations in Fig. 9 are even low-damped, representing a risk for the stability. This behavior is correctly predicted by the eigenvalue analysis in Fig. 6, for which when the emulated inertia is too high (low ω_f), the system eigenvalues moves toward the imaginary axes. The frequency of these oscillations is low (around 10 Hz) in accordance with the eigenvalue analysis in Fig. 6.

V. EXPERIMENTAL RESULTS

The considered VSC, as shown in Fig. 1, is reproduced in the lab with a 10 kW converter controlled through MicroLabBox connected to a grid simulator according to Fig. 10. The dc power P_{dc} is generated by a rectifier connected in back-to-back configuration with the considered VSC. The hardware parameters of the experimental setup are listed in Table II. A voltage sag of 0.2 p.u. is simulated in four different case studies, each one with a different control parameters tuning expressed in Table III; the converter dynamic behavior in the four case studies is shown in Fig. 11. The three experiments of Fig. 11(a),(b),(c) have been carried out using tuning guidelines present in literature, without optimizing the whole control system by means of the eigenvalue analysis. Active and reactive power droops are tuned with the rules of frequency/voltage deviations [20]. Oscillations with different frequencies and damping arise in these experiments, revealing a low dynamics damping, potentially dangerous for the stability. In Fig. 11(d), the tuning of

the control loops is optimized by means of the complete state-space model (3)-(4), according to the procedure of section III. Oscillatory phenomena due to control loops interactions are therefore avoided. The result is a fast response without low damped oscillations, confirming the effectiveness of the proposed tuning method.

VI. CONCLUSIONS

The main findings and achievements of this research can be summarized as:

- The interaction mechanisms among synchronization, dc voltage control and reactive power control in power synchronization-based converter have been described.
- A tuning guideline for the PI dc voltage control cascaded with frequency droop is proposed. The existing guideline in [3], published in 2019, considers P dc voltage control.
- The tuning method proposed in this paper considers all the loops interactions. Most of the control tuning guidelines in literature focus on a limited number of dynamics and control loops. The paper [8] considers the interaction of a wide number of control loops, but neglects the dc voltage dynamics and control, while [3] does not consider the reactive power loop.

REFERENCES

- [1] Q.-C. Zhong and G. Weiss, "Synchronverters: Inverters that mimic synchronous generators," *IEEE Transactions on Industrial Electronics*, vol. 58, no. 4, pp. 1259–1267, 2010.
- [2] L. Zhang, L. Harnefors, and H. Nee, "Power-synchronization control of grid-connected voltage-source converters," *IEEE Transactions on Power Systems*, vol. 25, no. 2, pp. 809–820, 2010.
- [3] L. Harnefors, M. Hinkkanen, U. Riaz, F. M. M. Rahman, and L. Zhang, "Robust analytic design of power-synchronization control," *IEEE Transactions on Industrial Electronics*, vol. 66, no. 8, pp. 5810–5819, 2019.
- [4] J. Liu, Y. Miura, and T. Ise, "Comparison of dynamic characteristics between virtual synchronous generator and droop control in inverter-based distributed generators," *IEEE Transactions on Power Electronics*, vol. 31, no. 5, pp. 3600–3611, 2016.
- [5] S. D'Arco and J. A. Suul, "Equivalence of virtual synchronous machines and frequency-droops for converter-based microgrids," *IEEE Transactions on Smart Grid*, vol. 5, no. 1, pp. 394–395, 2014.
- [6] J. Fang, H. Li, Y. Tang, and F. Blaabjerg, "Distributed power system virtual inertia implemented by grid-connected power converters," *IEEE Transactions on Power Electronics*, vol. 33, no. 10, pp. 8488–8499, 2017.
- [7] T. Wu, Z. Liu, J. Liu, S. Wang, and Z. You, "A unified virtual power decoupling method for droop-controlled parallel inverters in microgrids," *IEEE Transactions on Power Electronics*, vol. 31, no. 8, pp. 5587–5603, 2016.
- [8] S. D'Arco, J. A. Suul, and O. B. Fosso, "Automatic tuning of cascaded controllers for power converters using eigenvalue parametric sensitivities," *IEEE Transactions on Industry Applications*, vol. 51, no. 2, pp. 1743–1753, 2015.
- [9] F. Cecati, R. Zhu, M. Liserre, and X. Wang, "State-feedback-based low-frequency active damping for vsc operating in weak-grid conditions," in *2020 IEEE Energy Conversion Congress and Exposition (ECCE)*, 2020, pp. 4762–4767.

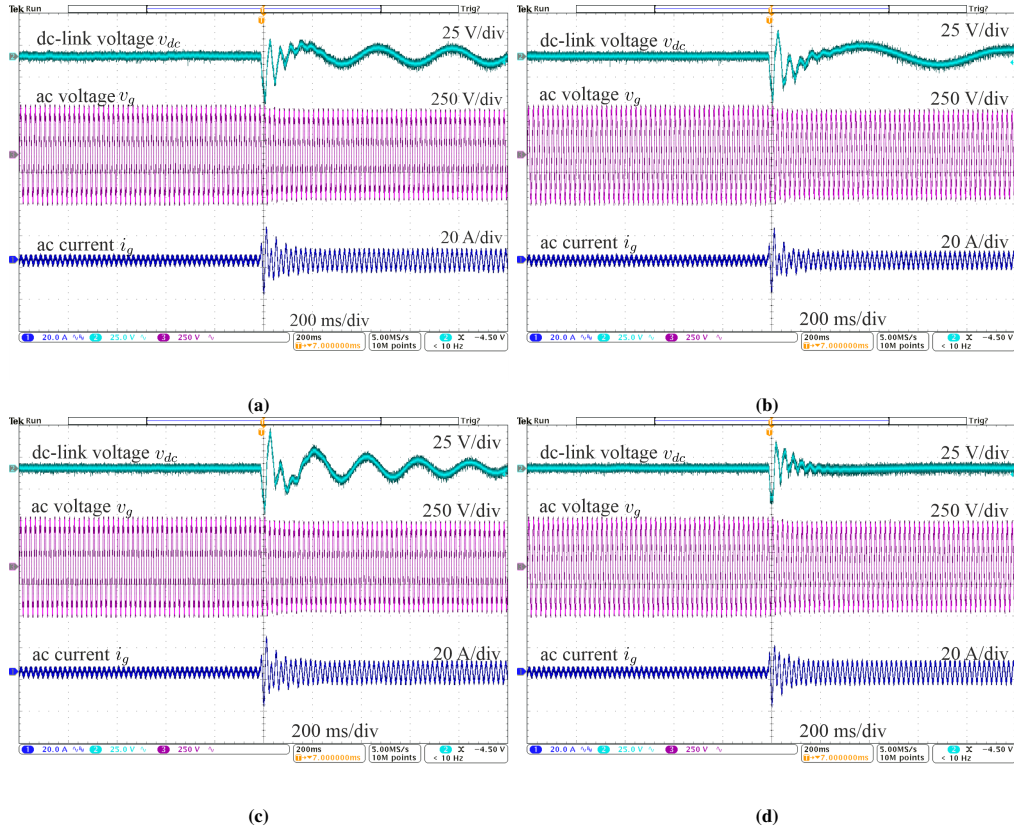


Figure 11: The experimental results with four different parameters tuning, reported in Table III. (a),(b),(c) Tuning realized according to different control parameters tuning without considering the control loops interactions. (d) Tuning realized through the proposed method.

- [10] F. Cecati, R. Zhu, M. Langwasser, M. Liserre, and X. Wang, "Scalable state-space model of voltage source converter for low-frequency stability analysis," in *2020 IEEE Energy Conversion Congress and Exposition (ECCE)*, 2020, pp. 6144–6149.
- [11] F. Cecati, M. Andresen, R. Zhu, Z. Zou, and M. Liserre, "Robustness analysis of voltage control strategies of smart transformer," in *IECON 2018 - 44th Annual Conference of the IEEE Industrial Electronics Society*, 2018, pp. 5566–5573.
- [12] N. Pogaku, M. Prodanovic, and T. C. Green, "Modeling, analysis and testing of autonomous operation of an inverter-based microgrid," *IEEE transactions on Power Electronics*, vol. 22, no. 2, pp. 613–625, 2007.
- [13] R. Rosso, S. Engelken, and M. Liserre, "Current limitation strategy for grid-forming converters under symmetrical and asymmetrical grid faults," in *2020 IEEE Energy Conversion Congress and Exposition (ECCE)*, 2020, pp. 3746–3753.
- [14] Y. Li, J. Guo, H. Wu, X. Wang, B. Zhao, S. Wang, and G. Wu, "Voltage stability and transient symmetrical fault current control of voltage-controlled mmcs," *IEEE Transactions on Power Delivery*, vol. 35, no. 5, pp. 2506–2516, 2020.
- [15] S. Yang, J. Fang, Y. Tang, H. Qiu, C. Dong, and P. Wang, "Modular multilevel converter synthetic inertia-based frequency support for medium-voltage microgrids," *IEEE Transactions on Industrial Electronics*, vol. 66, no. 11, pp. 8992–9002, 2019.
- [16] A. E. Leon, "Short-term frequency regulation and inertia emulation using an mmc-based mtdc system," *IEEE Transactions on Power Systems*, vol. 33, no. 3, pp. 2854–2863, 2018.
- [17] M. Saunders, P. Lewis, and A. Thornhill, "Research methods," *Business Students 4th edition Pearson Education Limited, England*, 2007.
- [18] R. C. Dorf and R. H. Bishop, *Modern Control Systems*. Pearson, 2011.
- [19] R. Teodorescu, M. Liserre, and P. Rodriguez, *Grid Converters for Photovoltaic and Wind Power Systems*. John Wiley & Sons, 2011, vol. 29.
- [20] J. C. Vasquez, J. M. Guerrero, M. Savaghebi, J. Eloy-Garcia, and R. Teodorescu, "Modeling, analysis, and design of stationary-reference-frame droop-controlled parallel three-phase voltage source inverters," *IEEE Transactions on Industrial Electronics*, vol. 60, no. 4, pp. 1271–1280, 2013.